Edge Stochastization and Collisionality Dependence of the L-H Power Threshold with Applied n=3 Resonant Magnetic Perturbations

L. Schmitz,[1] D.M. Kriete,[2] R.S. Wilcox,[3] T.L. Rhodes,[1] L. Zeng,[1] Z. Yan,[2] G.R. McKee,[2] T.E. Evans,[4] C. Paz-Soldan,[4] S.R. Haskey,[5] B.A. Grierson,[5] P.Gohil,[4] B. Lyons,[4] C.C. Petty,[4] D. Orlov[6]

[1]University of California Los Angeles, PO Box 957099, Los Angeles, CA 90095-7099, USA
[2]University of Wisconsin-Madison, 1500 Engineering Dr., Madison, WI 53706, USA
[3]Oak Ridge National Laboratory, Oak Ridge, TN 37831-0117, USA
[4]General Atomics, PO Box 85608, San Diego, CA 92186-5608, US
[5]Princeton Plasma Physics Laboratory, Princeton, NJ 08543-0451, USA.
[6]University of California San Diego, La Jolla, CA 920930417, USA.

Abstract: The stochastic edge magnetic field topology with applied resonant magnetic perturbations can explain the increased L-H power threshold [1,2] with applied n=3 resonant magnetic perturbations (RMP) in low rotation, ITER-similar-shape (ISS) plasmas in DIII-D. At low, ITER–relevant edge collisionality, the L-H power threshold is increased by a factor of almost three with respect to the Martin scaling. In this paper, reduced L-mode ***E×B*** shear with applied RMP is established as the likely cause of the increased L-H transition power threshold.

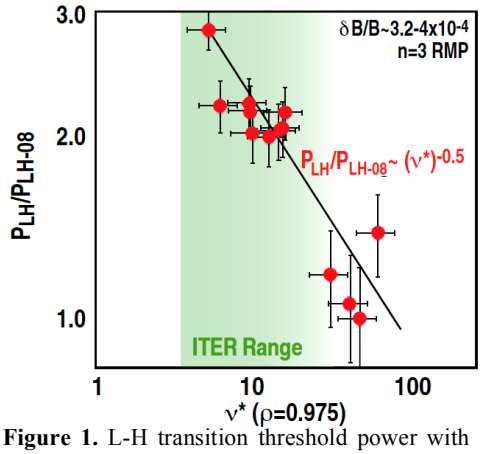

Figure 1. L-H transition threshold power with applied RMP, normalized by P_{LH-08}, the power threshold predicted by the 2008 ITPA Martin scaling, vs. edge plasma collisionality. The ITER L-mode edge collisionality range is indicated.

The effect of RMP on the L-H power threshold is investigated in ISS plasmas ($<n_e>$=1.5-5x10^{19}m^{-3}, B_t=1.9-2T, I_p=1.5 MA, q_{95}~3.6) with balanced neutral beam injection (toroidal beam torque < 0.1 Nm). ECH is added in a number of shots to increase edge electron temperature and reduce edge collisionality. With applied RMP, the normalized L-H transition power threshold in DIII-D is found to scale inversely with edge collisionality as $P_{LH}/P_{LH-08} \sim \nu_e^*(\rho=0.975)^{-0.5}$, where P_{LH-08} is the 2008 ITPA power threshold scaling (Martin scaling [3]; see figure 1). The dynamics of 3-D field- and rotation changes leading to reduced ***E×B*** shear in the presence of applied RMP are examined in figure 2 for an ISS L-mode plasma where n=3 RMP is applied at 1.2 s and then reduced step-wise. NBI and ECH power are kept constant. The ***E×B*** drift (shown for ρ~0.96 near the bottom of the L-mode E_r well) initially has a transient in the positive (ion diamagnetic drift) direction and then settles to a weakly negative value (in the electron diamagnetic direction) that is less negative than in the absence of RMP. Finite (intrinsic) toroidal edge rotation in the co-current direction is observed although the NBI torque is balanced. The ***E×B*** drift becomes more negative as the RMP coil current is stepped down, increasing edge ***E×B*** shear [2]. Concomitantly the edge fluctuation level [measured by Doppler Backscattering (DBD)] is reduced (shown in more detail in [2]), and the L-H transition is triggered finally after the second I-coil step-down (the increase of the ***E×B*** velocity after the transition is an artefact due to outwards displacement of the DBS probing radius, as the local density increases after edge transport barrier formation). In this case, with an edge collisionality $\nu_e^*(\rho=0.975)$ ~13.3, the L-H power threshold (the loss power across the separatrix) is about 2.8 MW.

These discharges reside close to a bifurcation point in edge radial electric field, as seen in figure 3 for nearly identical heating power and plasma parameters, where the edge ***E×B*** drift [fig. 3(a)] remains strongly positive after the RMP are applied [2,4], and concomitantly the toroidal edge

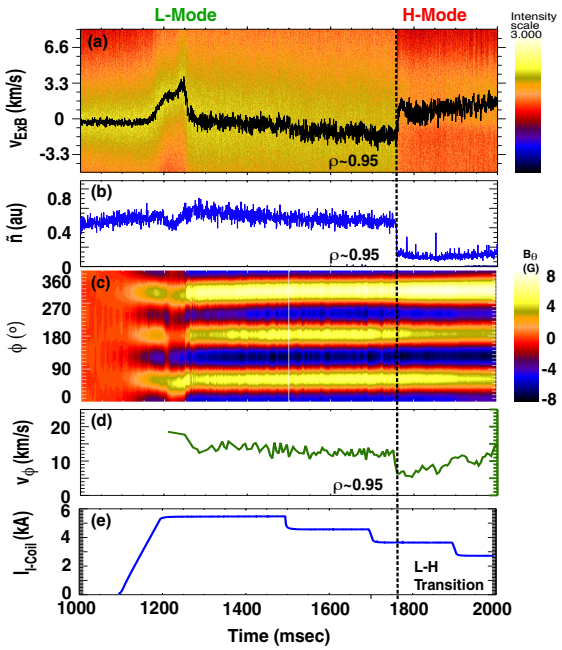

Figure 2. *Evolution of (a) **E×B** velocity from turbulence advection measured by DBS with applied RMP; (b) density fluctuation level ñ(ρ=0.95) for k_{perp} ρ_s ~ 0.5; (c) poloidal magnetic field from 3-D diagnostics; (d) toroidal edge rotation (ρ=0.95), and (e) I coil current waveform.*

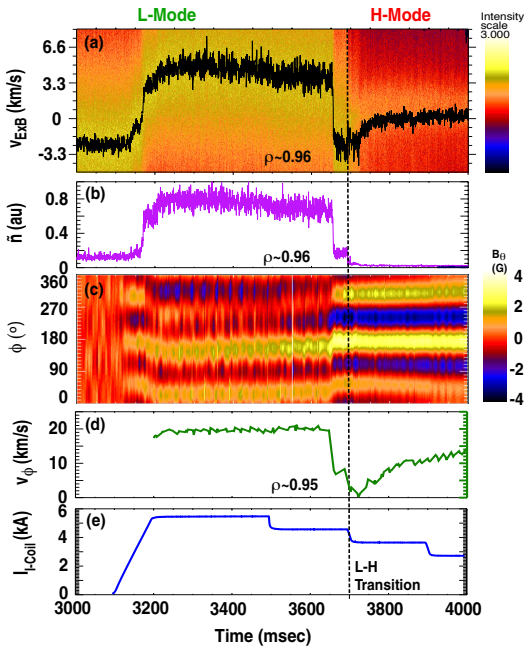

Figure 3. *Evolution of (a) **E×B** velocity by DBS with applied RMP (bifurcated case); (b) density fluctuation level ñ(ρ=0.95) for k_{perp} ρ_s ~ 0.5; (c) poloidal magnetic field from 3-D diagnostics; (d) toroidal rotation (ρ=0.95), and (e) I-coil current waveform.*

rotation is increased [fig. 3(d)]. With positive E_r, H-mode cannot be accessed at any collisionality for the heating power range explored here (≤4 MW). The density fluctuation level [fig. 3(b)] is substantially higher than in fig. 2(b). The L-H transition again occurs only after the I-coil current is reduced and the toroidal rotation drops [fig. 3(d)], and the edge electric field bifurcates back (within about ~3 ms) to negative polarity (at 3680 ms). Characteristic differences in the evolution of the toroidal mode structure of B_θ measured via a high-field-side 3-D coil array are observed. In fig. 2(c), the measured n=3 B_θ amplitude and phasing suggests n=3 field penetration and possibly n=3 mode locking when RMP are applied. In contrast, in fig. 3(c) the plasma response is clearly different with field penetration /n=3 mode locking suggested only at 3650 ms with reduced toroidal rotation, after the I-coil current is stepped down at 3500 ms. n=1,2 mode evolution (not shown) is also different in both cases and needs further investigation. Simultaneously the edge density fluctuation level decreases substantially [fig. 3(b)]. Shortly afterwards the I-coil current is further stepped down, $v_{\mathbf{E\times B}}$ becomes more negative (further increasing the local ***E×B*** shear), and the L-H transition is triggered

This difference in behavior can be explained if we consider stochasticity in the L-mode plasma edge before the L-H transition. The RMP perturbation strength and the expected island sizes have been evaluated based on a vacuum field calculation, and separately by taking into account the linear plasma response via the M3D-C1 code (including known n=1-4 field error field components due to coil geometry, coil buses etc.). Table I shows the expected relative perturbation field $\delta B_r/B$ calculated for different edge-resonant n=3 spectral components for the vacuum field, and including the linear plasma response. TRIP3D fieldline tracing calculations show a stochastic field line loss fraction of up to 90% for $\rho > 0.96$ with the plasma response included. Previous theory postulates that stochastic magnetic field lines diffuse with a characteristic diffusion coefficient D_{ST}, based on the Rechester-Rosenbluth model [5]. A simple fluid model based on stochastic edge electron transport [6,7,2], balancing stochastic radial electron flow and neoclassical ion flow, explains quantitatively the observed modifications of the toroidal rotation and E_r. Diffusion along braided fieldlines leads to an

effective electron stochastic conductivity that can be expressed for sufficiently high electron collisionality as $\sigma_{ST} = k_1 \sigma_{\parallel} D_{ST} / L_K$ where $\sigma_{\parallel} = ne^2 / m_e \nu_{ei}$ is the Spitzer parallel conductivity that introduces the collisionality dependence of the power threshold, $D_{ST} = [2\pi B / B_\theta](\delta B_r / B)^2$ is the quasilinear estimate for the stochastic fieldline diffusion coefficient [4], and $L_K \sim qR$ is the Kolmogorov length [7], with a parameter k_1 accounting for the stochastic field line loss fraction. The radial electron current that can flow to structures in the scrape-off layer due to stochasticity can then be expressed as [6,7]

$$j_r^e = \sigma_{ST}\left[E_r + \frac{T_e}{e}\frac{1}{n}\frac{\partial n}{\partial r} + 1.71\frac{1}{e}\frac{\partial T_e}{\partial r}\right]. \quad [1]$$

m/n	ρ	q	$\delta B_{r\,vac}/B$ [10^{-4}]	$\delta B_r/B$ [10^{-4}]
14/3	0.989	4.67	4.55	1.58
12/3	0.971	4.0	4.69	0.93
11/3	0.954	3.67	4.4	0.50
10/3	0.923	3.33	4.12	0.22
9/3	0.893	3.0	4.3	0.11

Table I. Resonant radii, local safety factor, relative vacuum radial magnetic field amplitude, and $\delta B_r/B$ calculated including the plasma response from the M3D-C1 code, for resonant n=3 harmonics outside of ρ=0.8.

Equating this current with the neoclassical radial ion current $j_r^i = \sigma_{Neo}\left[E_r - E_r^{Neo}\right]$, where $\sigma_{Neo} = (3/2)\mu_{i1}/R^2B^2$ is the neoclassical radial ion conductivity, E_r^{Neo} is the neoclassical electric field, and the ambipolar radial electric field in the presence of stochasticity is calculated as

$$E_r^{ST} = \left(\frac{\sigma_{Neo}}{\sigma_{Neo}+\sigma_{ST}}\right)E_r^{Neo} - \left(\frac{\sigma_{ST}}{\sigma_{Neo}+\sigma_{ST}}\right)\left[\frac{T_e}{e}\frac{1}{n}\frac{\partial n}{\partial r} + \alpha\frac{1}{e}\frac{\partial T_e}{\partial r}\right]. \quad [2]$$

Figure 4 shows the radial electric field E_r^{ST} based on this model (and the toroidal main ion velocity calculated from radial main ion force balance) for a reference case without applied RMP, and for cases with high applied RMP with and without bifurcation. Compared to the reference case without RMP [fig. 4(a) and (d)], at high applied RMP, E_r and the toroidal rotation increase in the edge plasma in figs. 4(b) and (e). The best match to the experimental (CER and DBS) data was obtained with a 15 cm radial e-folding length of the applied RMP perturbation $\delta B_r/B$. This decay length is consistent with TRIP3D predictions for the vacuum case, likely indicating that field penetration is important in this case. In the bifurcated case with positive edge E_r [hill structure, figs. 4(c) and (f)] the required e-folding length to obtain a match with the experimental data is 4.5 cm [vs. ~2 cm suggested by the M3D-C1 simulation (table I)], suggesting strong plasma screening of the RMP field. This is qualitatively consistent with the observed increased toroidal edge rotation, with the lower perturbations predicted by M3D-C1 when the plasma response is included, and with the lower B_θ response that is recorded in the 3-D magnetic field diagnostics [fig. 3 (c)]. Poloidal main ion rotation [fig. 4(g,h)] has been extracted from the electric field and the toroidal rotation determined via CER, and the main ion pressure gradient. It is assumed here that the main ion toroidal rotation and ion temperature can be approximated by the measured Carbon ion data. This data suggests that poloidal rotation may be comparable to toroidal rotation near the separatrix, but falls off substantially towards smaller radii, amounting to < 10% of the toroidal rotation at ρ=0.9. Figure 5 shows a comparison of the $\boldsymbol{E\times B}$ shearing rate extracted from CER measurements for the three cases discussed here. In figure 5(a) the Hahm-Burrell shearing rate is compared at four different normalized radii, demonstrating clearly that the shearing rate is reduced at high applied RMP both for the case with negative E_r and for the bifurcated case with positive E_r. Micro-instability growth rates for these cases have been calculated with the Trapped Gyro Landau Fluid (TGLF) linear stability code. Figure 5(b) shows a plot of the maximum linear growth rate γ_L normalized by the $\boldsymbol{E\times B}$ shearing rate $\omega_{\boldsymbol{E\times B}}$. The reduction of $\omega_{\boldsymbol{E\times B}}$ is most pronounced in the non-bifurcated case. The reduction of $\omega_{\boldsymbol{E\times B}}$ is most pronounced in the non-bifurcated case, hence $\gamma_L / \omega_{E\times B}$ increases most significantly in that case.

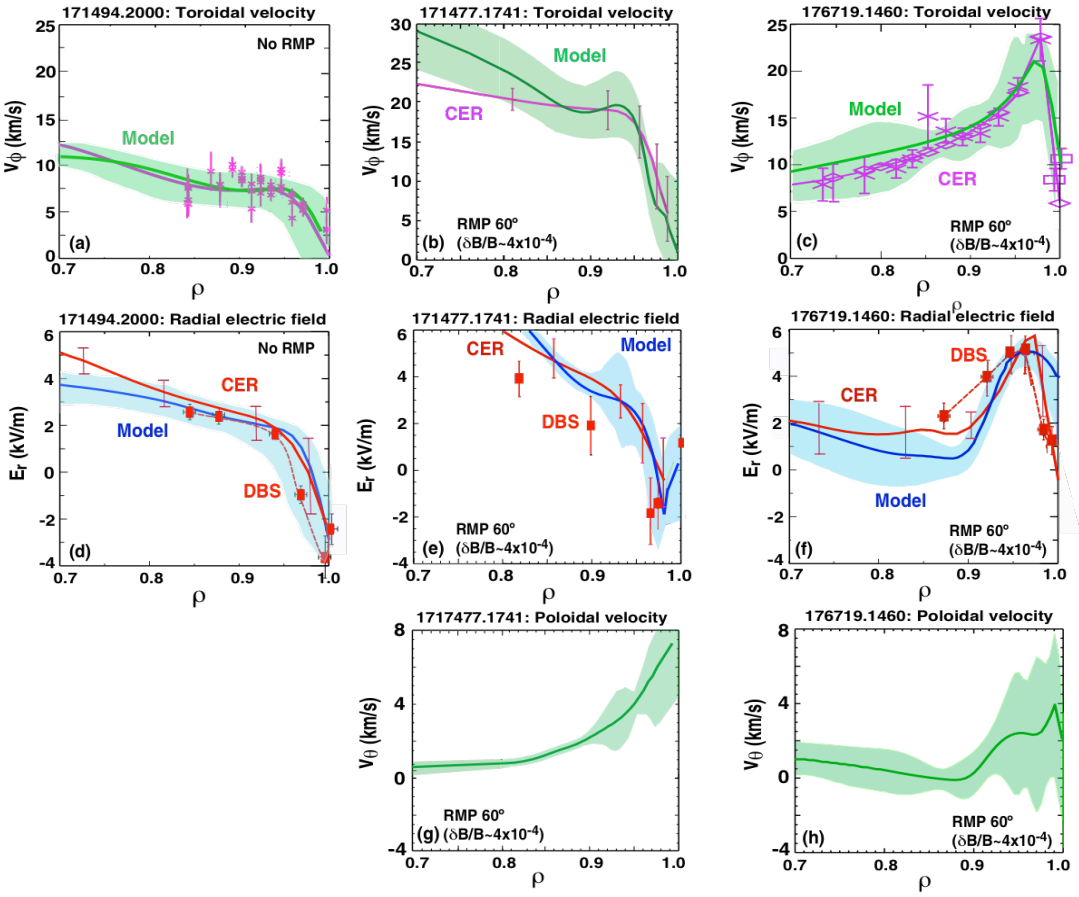

Figure 4. *(a) toroidal rotation, and (d) radial electric field E_r for a zero RMP reference shot; (b) toroidal rotation, (e) E_r, (g) inferred poloidal rotation profile with applied high RMP (non-bifurcated case); and (c) toroidal rotation, (f) E_r, and (h) inferred poloidal rotation for the bifurcated case.*

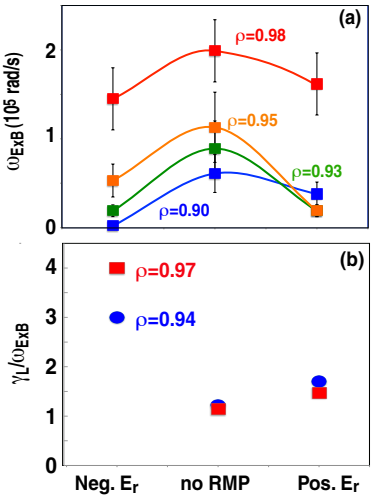

Figure 5. *(a) ExB shearing rate at four radii for conditions with zero RMP, high applied RMP ($\delta B_r/B \sim 4.4x10^{-4}$) but no electric field reversal, and bifurcated E_r ($\delta B_r/B \sim 4.4x10^{-4}$); (b) ratio of maximum linear instability growth rate γ_L from TGLF (for $k_\theta \rho_s \leq 1$) and the $\boldsymbol{E}\times\boldsymbol{B}$ shearing rate $\omega_{\boldsymbol{E}\times\boldsymbol{B}}$ for the same conditions ($<n_e>\sim 3\times10^{19} m^{-3}$; P_{NBI} =1.7MW, P_{ECH}~1 MW).*

In summary, the data presented here suggest that the increased L-H power threshold with RMP is caused by less negative E_r and reduced $\boldsymbol{E}\times\boldsymbol{B}$ shear with applied RMP. The observed E_r and rotation changes, both with RMP screening and with n=3 field penetration, are consistent with a model based on increased radial electron heat loss due to magnetic stochasticity.

*This material is based upon work supported by the U.S. Department of Energy, Office of Science, Office of Fusion Energy Sciences, using the DIII-D National Fusion Facility, a DOE Office of Science user facility, under Awards DE-FG02-08ER54984, DE-FG02-89ER53296, DE-FG02-08ER 54999, and DE-FC02-04ER54698. DIII-D data shown in this paper can be obtained in digital format by following the links at https://fusion.gat.com/global/D3D_DMP.

[1] P. Gohil, T.E. Evans, et al., Nucl. Fusion **51**, 030120 (2011).
[2] L. Schmitz, D.M. Kriete, R. Wilcox, T.L. Rhodes et al., submitted to *Nucl. Fusion.*
[3] Y.R. Martin ,T. Takizuka et al. 2008 *J. Physics: Conf. Series* **123** 012033.
[4] Mordijck S., Rhodes T.L., Zeng L., Doyle E.J., Schmitz L. et al. 2015 *Plasma Phys. Control. Fusion* **58** 014003.
[5] Rechester A.B. and Rosenbluth M. 1978 *Phys. Rev. Lett.* **40** 38.
[6] Kaganovich I. and Rozhansky V. 1998 *Phys. Plasmas* **5** 3901.
[7] Rozhansky V., Kaveeva E. and Tendler M. 2008 *Nucl. Fusion* **48** 075003.